Influence of bubble size on perfluorooctanesulfonic acid degradation in a pilot scale non-thermal plasma treatment reactor

David Alam [a], Samiuela Lee [a], Jungmi Hong [a], David F. Fletcher [a], Xinying Liu [a], Dale McClure [a,b], David Cook [c], Johan le Nepvou de Carfort [d], Ulrich Krühne [d], P.J. Cullen [a], John M. Kavanagh [a,d,*]

[a] School of Chemical and Biomolecular Engineering, The University of Sydney, 2006, Australia
[b] Department of Chemical Engineering, College of Engineering, Design and Physical Sciences, Brunel University, London, Uxbridge UB8 3PH, UK
[c] Ventia Australia Pty Ltd, North Sydney, NSW 2060, Australia
[d] PROSYS Technical University of Denmark Chemical and Biochemical Engineering, Kongens Lyngby 2800, Denmark

ARTICLE INFO

ABSTRACT

A 25L working volume non-thermal plasma-based treatment reactor was trialled to destroy per- and poly-fluoroalkyl substances (PFAS) utilising argon bubbles to transport PFAS to the surface to be destroyed with plasma interaction at the argon-liquid interface. The breakdown rate of PFAS and the system's overall energy efficiency could be improved while minimising gas usage by utilising small bubbles (0.6–0.7 mm d_{32}) to maximise the transport of PFAS to the plasma discharge for destruction. Vertically scaling the treatment reactor dimensions increases the overall liquid height and dwell time for bubbles to contact and transport PFAS molecules to the surface. The removal rate of perfluorooctane sulfonate (PFOS) correlated with the total surface area of the gas. Significant concentration gradients of PFOS could be observed when sampling from different liquid heights within the 25 L reactor. A one-dimensional model of mass transfer to the surface of rising bubbles was developed and gave good predictions of the overall rates of PFOS breakdown with modelled time constants of 0.14–0.18 min^{-1} versus 0.16 ± 0.01 min^{-1} for the fine bubble diffuser, and 0.048–0.053 min^{-1} versus 0.06 min^{-1} for the medium bubble diffuser. The time constant compared favourably with similar experiments at the 2 L scale of 0.11 min^{-1}.

Nomenclature

a	Area per unit volume [m^{-1}]
A_b	Area of a single bubble [m^2]
C_{bl}	Concentration in the liquid at the bubble surface [kg m^{-3}]
C_{surf}	Bubble surface concentration [kg m^{-2}]
C_∞	Bulk concentration of PFOS in the liquid [kg m^{-3}]
C^*	Dissolved gas concentration at bubble surface [kg m^{-3}]
d_b	Bubble diameter [m^3]
H	Liquid height above the sparger [m]
K_{equil}	C_{surf}/C_{bl} is the equilibrium constant [m]
k_b	Breakdown rate [s^{-1}]
k_L	Liquid mass transfer coefficient [m/s]
m_b	Mass of PFOS on a single bubble [kg]
OTR	Oxygen Transfer Rate [kg m^{-2} s^{-1}]
P	Electrical power [W]
T	Time for initial concentration to be reduced by 90% [s]

(continued on next column)

Nomenclature *(continued)*

t	Time [s]
t_{rise}	Time for a bubble to travel from the sparger to the fee surface [s]
u_L	Bulk liquid speed [m/s]
u_b	Bubble terminal velocity [m/s]
V	Volume of fluid in the tank [m^3]
$\dot{V}_G$	Volumetric flowrate of argon gas [m^3/s]
Δt	Timestep [s]

1. Introduction

Per- and poly- fluoroalkyl substances (PFAS) are a diverse class of synthetic, organofluorine compounds that contain either completely fluorinated (perfluorinated alkyl substances) or partially fluorinated (polyfluorinated alkyl substances) alkyl chains [1]. Due to the highly electronegative nature of fluorine, carbon–fluorine bonds are extremely

strong allowing many PFAS to exhibit exceptionally high thermal and chemical stability [2,3]. The carbon–fluorine bond does not readily degrade by biological processes due to its stability, resulting in PFAS remaining in perpetuity in the environment and earning the moniker "Forever Chemicals" [4].

Many of these compounds are used in consumer applications to impart water and stain resistant coatings for textiles, non-stick cookware and floor polishes, and industrially as surfactants, emulsifiers, wetting agents, additives, and coatings [3]. While over 12,000 compounds are classified as PFAS by the United States Environmental Protection Agency (US EPA) PFASMASTER chemical database [1], research attention has primarily focussed on perfluorooctanoic acid (PFOA) and perfluorooctanesulfonate (PFOS) which have been formally classified as persistent organic pollutants (POPs) due to their recalcitrance and ubiquitous detection in the environment [3,5,6]. In addition to environmental persistence, these particular compounds can also bioaccumulate, and several probable links between adverse health effects due to PFAS exposure in humans have been observed, including kidney and testicular cancer, elevated cholesterol, pregnancy-induced hypertension, thyroid problems, hormone irregularities, and ulcerative colitis [7–9]. Given the persistence and ubiquitous nature of PFAS contamination, it is crucial to develop treatment strategies to remediate contamination by PFAS to protect the public's health and the environment.

Current remediation practices for PFAS contaminated sites or drinking water sources focus on removing the PFAS by adsorbing the molecules onto either granular activated carbon (GAC) or ion exchange resins. Other techniques such as foam floatation are also gaining popularity in concentrating PFAS into a low volume waste [10–12]. These techniques are effective at removing PFAS from contaminated water sources but require additional post-treatment steps, such as thermal treatment of PFAS laden adsorbents or thermal plasma treatment of foam concentrates.

The use of non-thermal plasma in PFAS remediation involves the generation of reactive species that can break down the carbon–fluorine bonds present in PFAS molecules. A range of different plasma interface strategies have been trialled in the literature. However, the most efficient reactor types exploit the surfactant-like properties of PFAS, to enrich the surface concentration by using bubbles to transport the PFAS to the gas–liquid interface to be exposed to a plasma discharge [13]. This treatment strategy can be operated at ambient temperature and pressure and has shown potential for treating large volumes of contaminated water at an increasingly larger scale (up to 300 L volume reactors) [14]. Researchers working on foam fractionation have demonstrated that the performance depends on the tendency of the PFAS compounds to adsorb to the bubbles and that the performance can be improved by the addition of cationic surfactants [10,15].

This treatment approach exploits the strong surfactant nature of PFAS by rising bubbles, accumulating them at the gas–liquid interface and enriching the localised concentration of PFAS by several orders of magnitude [13]. The adsorption of the PFAS species to the gas–liquid interface of the bubble is favoured by the presence of salts [17]. The plasma discharge then directly exposes the PFAS at the liquid surface to the introduced short lived radical species and solvated electrons in the water, and bombards the surface with highly energetic ionised gaseous species which can further facilitate breakdown [14].

The plasma exposes the enriched PFAS at the surface to highly active radical species (OH^-, $O_2^{\bullet-}$, O, H) and solvated electrons (e_{aq}^-), which can mineralise PFAS via reductive pathways [16–19]. Additionally, with sufficient energy input, the plasma channel can reach sufficiently high temperatures (> 2000 K), to achieve thermal decomposition of PFAS [20]. The destruction of PFAS by exposure to plasma at the gas–liquid interface occurs at an extremely short time scale as the reactive species involved, including solvated electrons and metastable plasma radicals, are short lived (10^{-9}-10^2 s) and readily interact and destroy PFAS accumulated at the interface. Researchers at Clarkson University have

developed models for plasma treatment of water, determining first order rate constants and the effects of discharge frequency in a shallow reactor, and identifying conditions that are limited by mass transfer and plasma power input [21,22].

Whilst the effects of operating parameters can be described qualitatively, there are not yet design equations in the open literature which can be used for designing plasma systems for PFAS destruction. To model this process, details of the bubble size distribution and gas velocity are needed, however, accurately measuring bubble size distribution (BSD) at significant gas flowrates is challenging. Optical methods are useful for low numbers of bubbles, but opacity and image processing limit their applicability. Electrical methods have been used for high bubble fractions, but these methods are generally limited to bubble sizes greater than 2 mm. Indirect measurements, such as oxygen transfer rates, measure the combined mass transfer coefficient for oxygen and the specific surface area [23]. From this quantity it is possible to estimate the average bubble size. It also has the advantage of directly measuring mass transfer rates which can then be scaled based on the relevant compounds diffusivity compared with that of oxygen.

In our previous work we demonstrated that the destruction of PFAS molecules in a 2 L, 0.13 m tall reactor, correlated with their tendency to adsorb to the bubble liquid interface [24]. In this work we test whether using smaller bubbles and a taller column could increase the efficiency of PFOS degradation. Understanding and controlling the optimal bubble size and hydrodynamics throughout a treatment reactor are therefore crucial parameters to optimise the overall transport of PFAS to the surface for destruction by plasma.

2. Materials and methods

2.1. 25 L Treatment Reactor Design Details

The body of the 25 L reactor, shown schematically in Fig. 1, consisted of a 650 mm long section of 250 mm OD, 240 mm ID acrylic tubing with six access ports to allow for liquid sampling, to insert the ground electrode inside the reactor, and to connect the diffuser to the gas supply. Either an ECD200 "fine bubble" diffuser from Enviroceramic (Ireland) or a corundum, disc shaped, "medium bubble" diffuser (150 mm × 15 mm thick Zongle (China)) was used to generate the bubbles. The diffuser sparged argon gas (99.999% purity) was supplied by an Alicat (USA) mass flow controller at a flow rate of 1.0 L/min (superficial velocity of 2.2 cm/s). Argon was used for bubbling to ensure the head space gas where the plasma discharge occurs was argon. A pressure of ~ 1.5 bar was required for the fine bubble diffuser, whereas the medium bubble diffuser operated at ~ 0.2 bar. The total liquid height in the reactor was ~ 580 mm when filled with 25 L of liquid and with the liquid displacement of the diffuser and holdup volume of the bubbles.

Liquid samples could be drawn manually from any of the three sampling points up the column wall, labelled B, C or D, by opening the respective needle valve and collecting ~ 30 mL in a high-density polyethylene (HDPE) sampling bottle. These sampling points B, C and D corresponded to liquid heights of 500 mm, 300 mm, and 100 mm as measured from the bottom of the reactor. Liquid samples could also be taken from the liquid surface by adjusting the height of a 6.35 mm stainless steel tube to be in contact with the surface to siphon liquid at sampling point A using a 50 mL syringe which was filled and emptied several times back into the reactor before collecting the sample. A WT600F intelligent dosing peristaltic pump from Leadfluid (China) was used to fill the reactor with 25 L of liquid (± 0.5%) via the 1/2" ball valve located at the base of the reactor. The reactor contents after the experiments were similarly decanted from the reactor into waste containers using the same valve and pump.

A 175 mm long, 3.2 mm OD, sharpened tungsten rod was used as the discharge electrode. The electrode was positioned at the centreline of the reactor and was supported ~ 12–15 mm above the liquid surface. The electrode height was adjusted during the experiment to maintain a
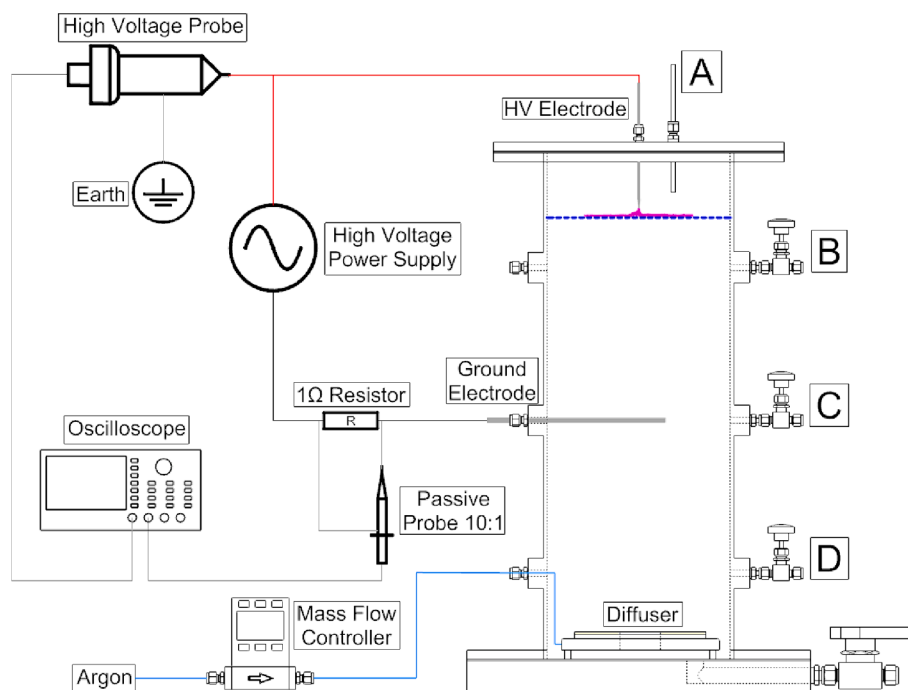
Fig. 1. Schematic diagram of the 25 L plasma treatment reactor.

consistent gap distance within this range as the liquid level in the reactor decreased over time due to sampling. A 300 mm long, 1/4" stainless steel rod was used as the ground electrode, and secured through the port opposite sample position C. The liquid remained at ambient temperatures between 22–25 °C over the 120 min of plasma treatment and the reactor did not require any cooling.

A high-voltage pulse generator model KAM-PGS05 from Kamea (Slovakia), was used to generate the high energy electrical pulses required to form a network of filamentous plasma which was estimated to interface with an area equivalent to at least 180 mm circle on the liquid surface and possibly the entire surface. The power supply could produce high-voltage pulses between 1–2.3 J at an adjustable pulse frequency between 100 to 1000 Hz. For these experiments, values of 2 J of energy per pulse at a pulse frequency of 200 Hz were used, with the discharge efficiency of the capacitors averaging ∼ 70% during experiments.

2.2. Electrical diagnostics

A model DS6104 4-channel digital oscilloscope from Rigol (China) was used with a PVM-6 high voltage probe from North Star High Voltage (USA) to measure the voltages and current during discharge. The discharge current of the plasma was determined by measuring the voltage drop across a 1 Ω aluminium-housed, wire-wound resistor using a 10:1 passive probe connected in series to the return wire to the KAM high-voltage power supply. An RP5600A passive high-resistance probe from Rigol with a 10:1 attenuation ratio was connected to each side of the resistor to measure the voltage drop across a known resistance value which allowed for the current of the plasma discharge to be determined based on Ohm's law. The 600 MHz bandwidth of the probe provided a sufficiently fast response time and high accuracy to provide high resolution of the current waveform over the nanosecond (1×10^{-9} s) range.

2.3. Chemicals

Aqueous stock solutions of PFOS were prepared on a mass basis to a concentration of ∼ 80,000 μg/L using perfluorooctanesulfonic acid (PFOS, ∼ 40% in H_2O) sourced from Sigma Aldrich (Australia) and high

purity, deionised water. The stock solutions were then spiked into the liquid pumped into the reactor while it was filled to homogenise the solution. The aqueous matrix added into the reactor was prepared with added calcium chloride to have a conductivity of 300 ± 1 μS/cm prepared with reverse osmosis water.

2.4. Liquid chromatography tandem mass spectrometry (LC-MS/MS)

A Thermo Scientific (USA) TSQ Altis triple quadrupole mass spectrometer was used to analyse liquid samples by liquid chromatography tandem mass spectrometry (LC-MS/MS). A gradient elution method was used with a binary mixture of: (A) 97.9% H_2O, 2% methanol, 0.1% acetic acid and 2 mM ammonium acetate and (B) 97.9% methanol, 2% H_2O, 0.1% acetic acid and 2 mM ammonium acetate. The gradient elution method used a total flowrate of 0.3 mL/min and was described in detail in our previous work [24]. Samples were spiked with an internal reference standard of C^{13} mass labelled PFAS standard mixture and injected without prior filtration. Concentrations were determined using calibration curves prepared with a native PFAS precision and recovery standard solutions.

2.5. Bubble size characterisation – Size distribution and mass transfer rates

A detailed overview of the photographic bubble size methodology employed at the University of Sydney is provided in the supplementary information in our previous work [24]. Briefly, the images of the bubbles produced by each respective diffuser were enhanced to improve contrast between bubbles and the background using Fiji (ImageJ, Version 2.9.0) software. The Weka Segmentation Algorithm was trained to identify bubbles. For the fine bubble sparger occasional bubbles with a diameter of 2 mm or more were produced at the intersection of the plastic backing sheet and the sparger which is an artefact of the measurement. The image processing algorithm also made measuring bubbles with a diameter less than 0.2 mm difficult due to limitations with differentiating these small bubbles versus visual artifacts.

The larger bubbles ∼ 3.0 mm in diameter produced by the medium bubble diffuser appeared more ellipsoidal or wobbling in shape rather

than spherical [25]. To approximate the diameter of the bubbles, the bubble sizing approach assumed that the bubbles were spherical to allow for the volume and surface area of the bubbles to be calculated based on the calculations for a sphere, i.e., the equivalent diameter was calculated based on the projected area of the bubbles. Therefore, the resulting diameters presented for the medium bubble diffuser assume these larger bubbles are spherical, while their shape may be more elongated or ellipsoidal. The photographic bubble size measurements and all previous experiments were conducted at the University of Sydney.

Given the limitations of the photographic method for measuring small bubbles, the bubble size distribution was also measured using a Dantec Dynamics A/S (Denmark) ParticleSight E endoscopic imaging probe in a 240 mm inner diameter, 20 L bubble column located at the Technical University of Denmark (Denmark). The water used was a 50/50 mix of deionised water (1 μS/cm) and tap water (800μS/cm), giving an average conductivity of ~ 400 μS/cm. The bubble size distributions from a different ECD200 ceramic diffuser and a 150 mm diameter disc corundum sparger (Hailea, China) were used with the Dantec endoscopic imaging probe. Air was used for the bubble size measurements as argon was not readily available.

For the fine bubble diffuser, bubble size measurements were taken using the Dantec endoscope at an angle of 25-30° off the vertical approximately ~ 200 mm above the diffuser and 50–80 mm from the wall of the column. This allowed the bubbles to flow between the LED and the endoscopic camera sensor. For bubble size measurements, the data acquisition frequency was set to 900 Hz and 1000 frames in total were collected. The minimum eccentricity, defined as the minor axis divided by the major axis, was set to 0.63 for the fine bubble diffuser to eliminate the detection of bubble clusters. A total of 100,000 bubbles were observed which the Dantec in-built software identified as 19,000–33,000 unique bubbles. This endoscope position and set-up could not obtain representative samples for the medium bubble sparger as the larger bubbles (~ 2 mm) would bypass the aperture between the LED and the endoscopic camera.

For the medium bubble sparger, a modified rectangular plastic tub was used allowing the aperture of the probe to be located directly above a section of the sparger. The data acquisition frequency was again set to 900 Hz with a total of 2000 frames collected. Given the prevalence of large ellipsoidal bubbles, the minimum eccentricity was set to 0.25 and roundness to 50% which resulted in the detection of 100,000–120,000 bubbles and 9,200–12,400 unique bubbles.

Videos were reviewed for all measurements; for the fine bubble diffuser bubbles were revealed to grow on the surface of the camera before reaching a size at which they detached, these bubbles were typically 2 mm or larger and were a source of variability between measurements that led to the inbuilt software overestimating the mean bubble size. The medium bubble sparger produced a mix of small spherical and larger ellipsoidal bubbles. Two inbuilt Dantec analysis software modules were tested: Dantec Shadow Statistics which gives a distribution of every identified bubble in each individual frame captured, and Dantec Adaptive Shadow Tracking, which assigns an identification number to each bubble characterised.

The ellipsoidal bubbles had a faster rise time, and this resulted in the inbuilt software underestimating the mean bubble size with the Shadow Statistics option. It was observed for both diffusers that the larger bubbles in the foreground could overshadow smaller bubbles in the background of the frames processed by the software, resulting in some of the smaller bubbles being given more than one unique identifying number.

The oxygen transfer rates (OTR) for each diffuser were measured using a small optical dissolved oxygen (DO) probe with fast dynamics from PyroScience GmbH (OXROB10, Germany) using the previously described 240 mm diameter, 20 L tank used for the bubble size measurements. The procedure for measuring the OTR was to deoxygenate the tank by sparging nitrogen until the DO levels were reduced below 1.5 mg/L. Once DO levels reached below this value, the nitrogen

supplied to the diffusers was stopped and replaced with air. The response of the DO over time was measured using the optical DO probe which had a measured response time of 3–4 s. Pointing the probe upwards reduced the attachment of bubbles to the probe, as these produce spurious readings approaching saturation. The volumetric mass transfer coefficient $k_L a$ was determined by fitting the OTR equation and minimizing the square of the errors between the measured and predicted results. The DO measurements over time for each sparger were made in triplicate. The OTR and DO concentrations are obtained from the following equations:

$$OTR = k_L a(C^* - C) \tag{1}$$

and

$$C_t = C_{t-1} + \Delta t \times k_L a(C^* - C_{t-1}) \tag{2}$$

The liquid film mass transfer coefficient can then be estimated for oxygen based on the bubble size determined previously, alternatively published relationships between the bubble size and the liquid film mass transfer coefficient can be used to determine the likely bubble size from the $k_L a$ value.

2.6. PFAS adsorption models

The PFAS adsorption model of Brusseau et al. was applied as the concentrations are sufficiently low to be in the linear range [26]. The adsorption coefficient for PFOS was 23 μm and PFOA 2.3 μm, a uniform enhancement of 74 was used for the presence of calcium ions in the water, resulting in surface concentration coefficients of 0.0017 m for PFOS and 0.00017 m for PFOA.

2.7. Liquid film mass transfer models

Motarjemi and Jameson measured oxygen transfer from small bubbles in water over a similar size range of interest as this study (0.1–3 mm) [27]. Motarjemi and Jameson found that the correlations of Frossling [28] and the small bubble correlation of Calderbank and Mooyoung [29] were suitable for bubbles of around 0.1 mm, whilst for 3 mm bubbles the equation of Higbie [30] or the large bubble correlation of Calderbank and Mooyoung were appropriate [27]. As the bubble sizes used in this study largely fell in an area where the most commonly used correlations are not applicable, the data from Motarjemi and Jameson were used to create a simple polynomial fit to k_L with bubble size over the range 0.5 to 3 mm [27].

3. Results and discussion

3.1. Fractionation of PFAS to the Surface

The composition of PFAS throughout the reactor before starting plasma treatment, given in Fig. 2, shows that the detected concentrations of PFAS increased with height in the reactor, forming gradients from sampling points D to A for both diffusers. This phenomenon was more pronounced for the fine bubble diffuser with PFOS concentrations detected at the liquid surface (136.5 μg/L) 200 to 300% higher when compared with the concentrations detected in samples from B, C and D (47.8, 41.6 and 38.7 μg/L) taken at differing heights from the bulk of the liquid. By comparison, the concentrations of PFOS exhibited reduced fractionation when operating with the medium bubble diffuser, which enriched the surface concentration at A (55.5 μg/L) by a modest 13 to 23% compared with liquid samples taken from the bulk of the liquid at B, C and D (48.8, 47.6 and 45.3 μg/L). The less prominent concentration gradients when operating with the medium bubble diffuser indicate the larger bubble size distribution was less effective in transporting the PFOS vertically but more effective at recirculating liquid throughout the reactor and homogenising the concentrations. Trace quantities of other
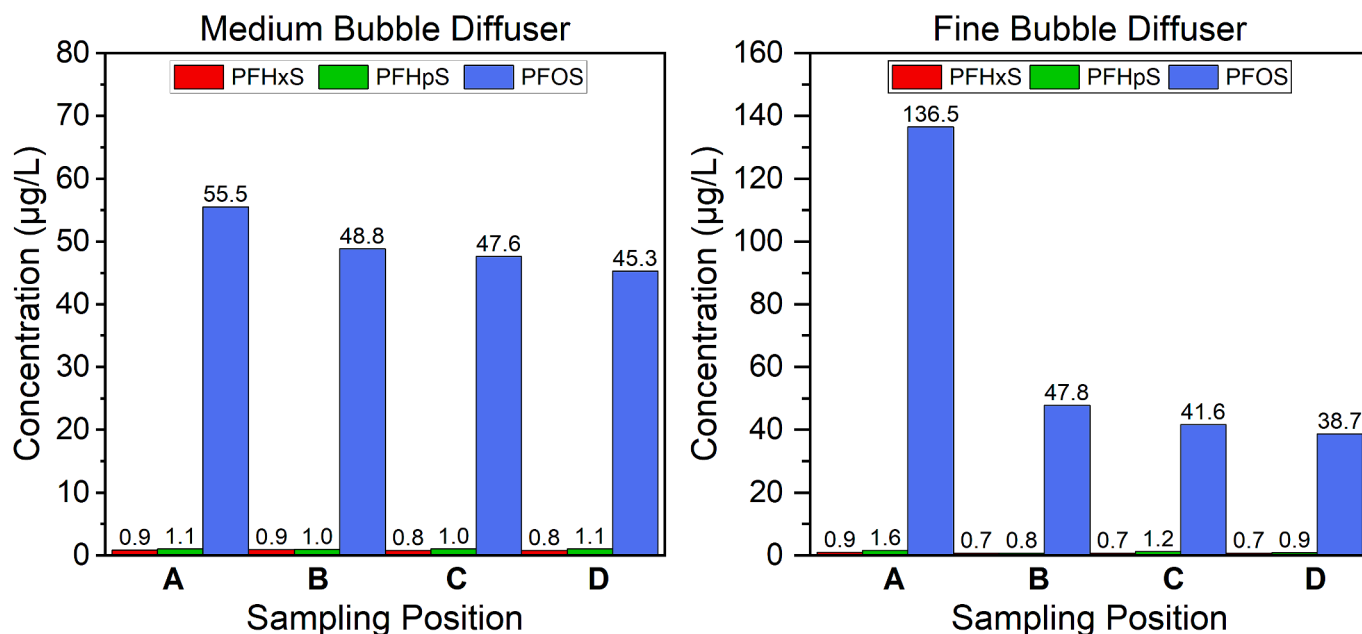
Fig. 2. Initial concentration of PFOS, PFHpS and PFHxS detected in the reactor when operating with the medium (left) and fine bubble (right) diffusers from liquid samples taken at different heights throughout the volume of the reactor.

perfluorocarboxylic acids (PFCA) containing 4 to 8 carbons, including perfluorobutanoic acid (PFBA), perfluoropentanoic acid (PFPeA), perfluorohexanoic acid (PFHxA), perfluoroheptanoic acid (PFHpA) and perfluorooctanoic acid (PFOA), were also initially detected throughout the reactor in trace quantities amounting to a total of < 0.4 μg/L.

The overall changes in PFOS concentrations at each time point were normalised with respect to the concentrations detected initially at each of the sample points A, B, C and D to compare the performance of both the medium bubble (left) and fine bubble (right) diffusers, as shown in Fig. 3.

Despite a reduced transport rate of PFOS to the surface compared with the smaller bubbles produced by the fine bubble diffuser, the larger bubble distribution from the medium bubble diffuser was still effective at transporting PFOS towards the liquid surface for destruction by the plasma. The concentration of PFOS was reduced by 98 to 99.5% after

120 min of plasma treatment, with < 0.25 μg/L detected throughout the reactor (B, C and D) and 1.2 μg/L at the liquid surface (A). The decrease in PFOS concentration throughout the reactor over time followed a pseudo-first order relationship on a logarithmic plot (supplementary information), indicating that the breakdown rate was limited by the transport of PFOS to the surface by attachment and flotation on the bubbles.

The time required to achieve a 90% decrease in PFOS concentration when operating with the medium bubble diffuser was significantly slower than the fine bubble diffuser. Using the medium bubble diffuser required ~ 40 min of plasma treatment to reduce the concentrations of PFOS by 90% for the bulk of the liquid (B, C and D) and > 60 min to reduce the concentration of PFOS by 90% at the liquid surface (A). These treatment times are 3–4 times longer when compared with the 13–16 min calculated when operating with the fine bubble diffuser, indicating
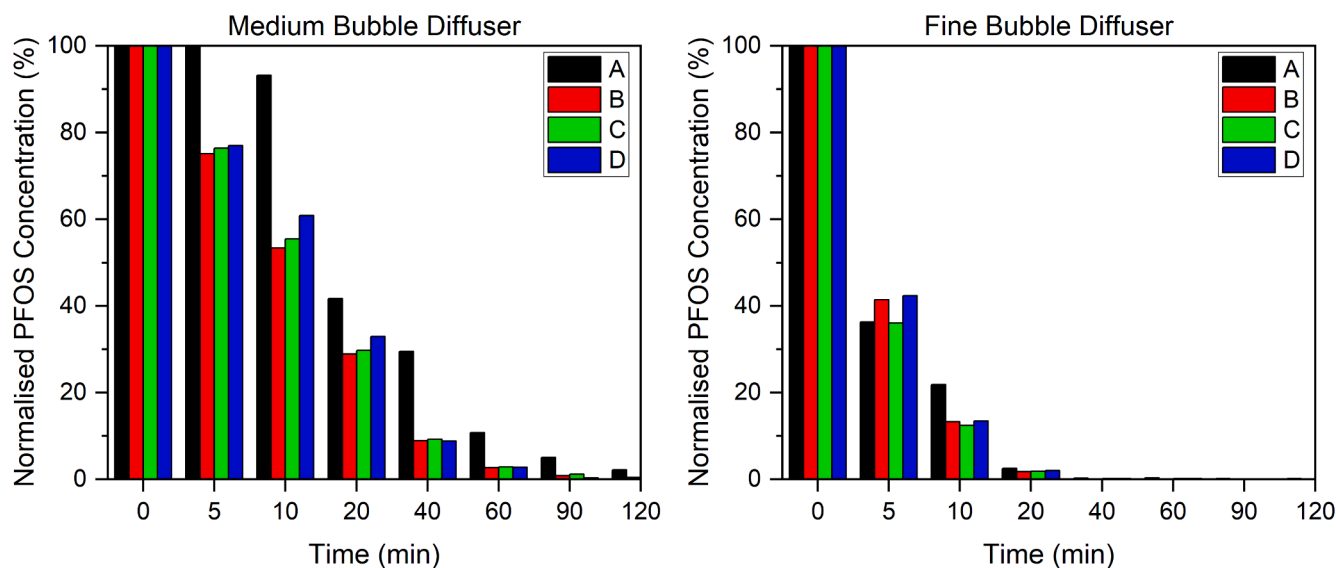

Fig. 3. Normalised PFOS concentrations detected from each of the sampling points A, B, C and D over time during plasma treatment between 0 to 120 min for both the medium bubble (left) and fine bubble (right) diffusers.

significant benefits in improving the degradation rate could be achieved by improving the floatation of PFAS to the surface by operating with smaller bubbles.

The data presented in Fig. 4 shows the concentration of each PFAS detected at sampling points A, B, C and D over the 120 min of plasma detected for both the fine bubble and medium bubble diffusers used. As can be seen in Fig. 4, rapid degradation and higher removal of PFOS was achieved, reaching a 100% reduction in concentration at all sampling points when comparing the initial concentration versus the final concentration after 120 min of plasma treatment for the fine bubble diffuser. After only 20 min of plasma treatment in the bulk of the liquid, PFOS could only be detected at C and D, and after 40 min of plasma treatment, no PFOS could be detected in the bulk of the liquid (B, C and D) with only trace quantities detected at the liquid surface (< 1 µg/L). After 40 min of plasma treatment and approaching 120 min treatment time, the concentration of PFOS in the liquid samples taken throughout the bulk of the liquid was effectively below the detection limits of the LC-MS/MS system (< 0.01 µg/L).

After the 120 min of plasma treatment, the remaining PFAS detected in the reactor consisted of a mixture of primarily C4 to C7 PFCA compounds detected at each of the four sampling points, except for PFOA, which was detected at 0.04 µg/L at sample point A, as shown Fig. 4. The

shorter chain PFCA compounds PFBA, PFPeA, and PFHxA were found to accumulate in the reactor and continuously increase in concentration over the 120 min of plasma treatment for both diffusers.

The reduced flotation efficiency of the medium bubble diffuser also reduced the destruction of several other compounds significantly, including PFHxS, PFHpS and PFOA. The shorter-chain PFSA, PFHpS and PFHxS were both impacted, with an average reduction in concentration of 92% and 43% after 120 min of plasma treatment, whereas the fine bubble diffuser achieved reductions > 98% after the same treatment time. The other recalcitrant, shorter chain PFCA (PFHpA, PFHxA and PFBA) were all observed accumulating and increasing in concentration over time. None of these compounds were observed to undergo any reduction in concentration compared with any initial concentration detected.

After 120 min of plasma treatment, the concentrations of key, regulated species, including PFOS (0.00 µg/L), PFOA (< 0.04 µg/L) and PFHxS (0.00 µg/L), were well below the current drinking water guidelines established by the Australian National Health and Medical Research Council (NHMRC) which recommend a maximum concentration of 0.07 µg/L for PFOS and PFHxS combined and 0.56 µg/L for PFOA [31,32]. Indeed, the concentration of these three key species reached below the concentrations defined in the drinking water quality
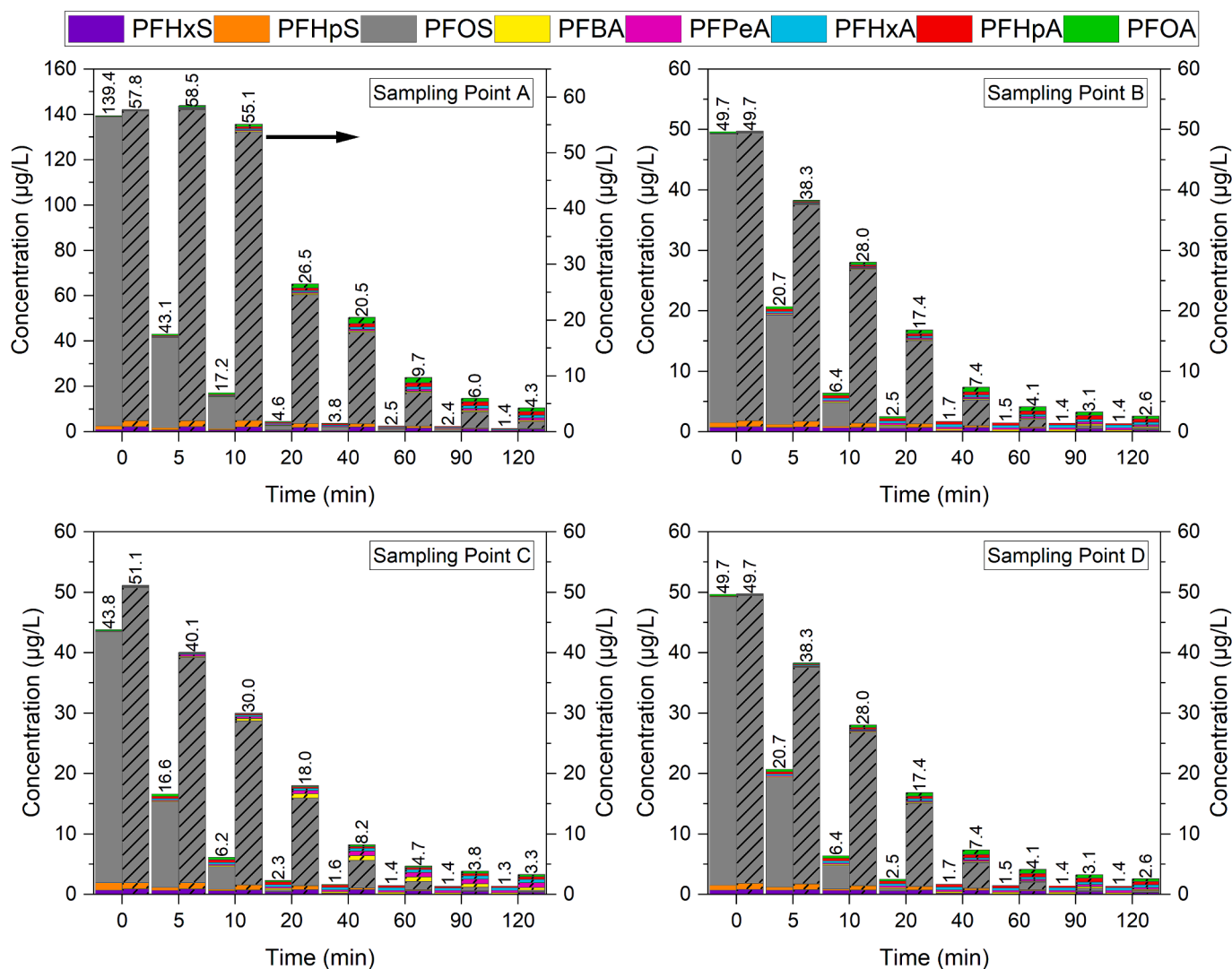

Fig. 4. Composition of PFAS detected at each time point during plasma treatment when utilising the fine (solid fill) or medium bubble diffuser (dashed). Note: different *Y* axis ranges for concentration between the plot for sampling point A (0–160 µg/L) compared with the other three plots for sampling points B, C and D (0–60 µg/L). The total concentration of PFAS detected at each time point is shown above each column.

guidelines after only 90 min of plasma treatment when considering the concentrations detected in samples taken from only the bulk of the liquid (B, C and D). However, the concentration of these key species at the liquid surface (sampling point A) exceeded the drinking water values defined by the NHMRC with a total of 0.98 μg/L of PFHxS (0.08 μg/L) and PFOS (0.90 μg/L). The variability in PFAS concentration from the bulk to the liquid surface in a tank raises an interesting design challenge for continuous systems to meet the low concentrations required for discharge or drinking water standards.

Additional cosurfactants could be added to enhance the fractionation effect and the overall removal rate of PFAS from contaminated water to enhance removal rates. Cationic surfactants have been shown to have the greatest benefit in improving the removal of negatively charged PFAS molecules from water by electrostatic interaction between the positively charged tail of the surfactant and the negatively charged functional group attracting the PFAS molecules to the liquid interface [33]. The addition of cationic surfactant cetrimonium bromide (CTAB) was trialled in an enhanced contact plasma treatment reactor sparging argon into the bulk liquid and discharging plasma to the surface to decompose the PFAS to increase the breakdown rate [34,35]. This approach improved the breakdown of PFAS; however, the process required six additions of CTAB over the 220 min treatment time to maintain the concentration at 0.2 mM (~73 mg/L) during the plasma treatment as the surfactant was prone to degradation by the plasma. It may be more effective to combine the plasma process here with an ion exchange or activated carbon process to meet the very low target values and as an insurance in case of poorer than expected removals.

Based on the results in Fig. 4, utilising the medium bubble diffuser and fine bubble diffusers, the breakdown rate of PFAS by the 25 L plasma treatment reactor appears to be limited by the transport of species to the liquid surface and plasma interface as utilising larger bubble sizes reduced the breakdown rate as a result of the reduced availability of surface area for PFAS species to attach to and float to the surface.

3.2. Electrical diagnostics and energy efficiency

A voltage and current waveform over a single pulse of energy supplied to the high-voltage electrode is shown in Fig. 5. The oscillations and intensity of the waveforms were consistent with a very high-powered burst of energy, reaching a peak-to-peak voltage of ~ 18 kV and a maximum current of ~ 150 A. The total duration of the pulse was ~ 1 ms; however, the primary current discharge event occurs over a much shorter time scale which can be seen more clearly in Fig. 5 (right), with a peak current of 115 A lasting < 40 ns.

An instantaneous peak power of approximately 1.36 MW was

calculated by integrating voltage and current waveforms with respect to time for these electrical pulses, with a total of 1.08 ± 0.03 J of energy consumed by the plasma discharge. From these values, the average power consumed over a second was determined to be 216.3 ± 6.6 W. The treatment reactor utilised only the industrial high voltage power supply and the mass flow controller (~10 W) to operate and no additional cooling was provided to the reactor as the liquid remained within the ambient temperature range of the laboratory (20 to 25 °C). The power consumption of the power supply and mass flow controller was determined to be 250 W, which was rounded up to account for any variability with measuring the power consumed by the power supply.

To benchmark and compare the effectiveness of this reactor with other treatment options, the Electric Energy per Order (EE/O) parameter was used to determine the energy requirements to achieve a 90% reduction in PFOS concentration in a 1 m^3 volume of PFAS-contaminated water.

$$EE/O = \frac{P \times T \times 1000}{V \times 60 \times \log(C_i/C_f)} \qquad (3)$$

where P is total power (kW), T is the time required to reach 90% reduction in PFOS concentration (min), V is the volume of liquid treated (L), and C_i and C_f are the initial and final concentrations of PFOS (μg/L). This parameter allows for the comparison of different advanced oxidation processes to compare their energy efficiencies for pollutant removal [36].

This parameter was calculated separately at each of the four-sampling points A, B, C and D, as each point had different initial and final concentrations of PFOS due to variability in the concentrations detected throughout the reactor volume. The average values were determined and the standard deviations were calculated utilising either the fine bubble or medium bubble diffuser. The values for each sampling point used to calculate the EE/O parameters have been included in the Supplementary Information Tables S1 and S2.

An average EE/O parameter of 1.6 ± 0.1 kWh/m^3 for remediating PFOS-contaminated water was determined for the fine bubble diffuser, whereas the medium bubble diffuser had a much higher EE/O of 8.4 ± 2.5 kWh/m^3. Compared with other plasma treatment reactor designs, the EE/O parameters calculated here are highly competitive. Singh et al. reported EE/O values of 1.7 to 6.3 kWh/m^3 for plasma treating nine different PFAS investigation-derived waters (IDW) containing a mixture of PFAS, including 0.1 to 21.8 μg/L PFOS [37]. The reactor in this work, however, utilised a 1:25 ratio of argon gas flow to water (1 L/min: 25 L of water), whilst the design used in Singh et al. used a higher ratio of 4 to 4.5:1 argon to water ratio (16 to 18 L/min: 4 L of water). To account for the different reactor geometries (tall cylindrical reactor vs shallow,
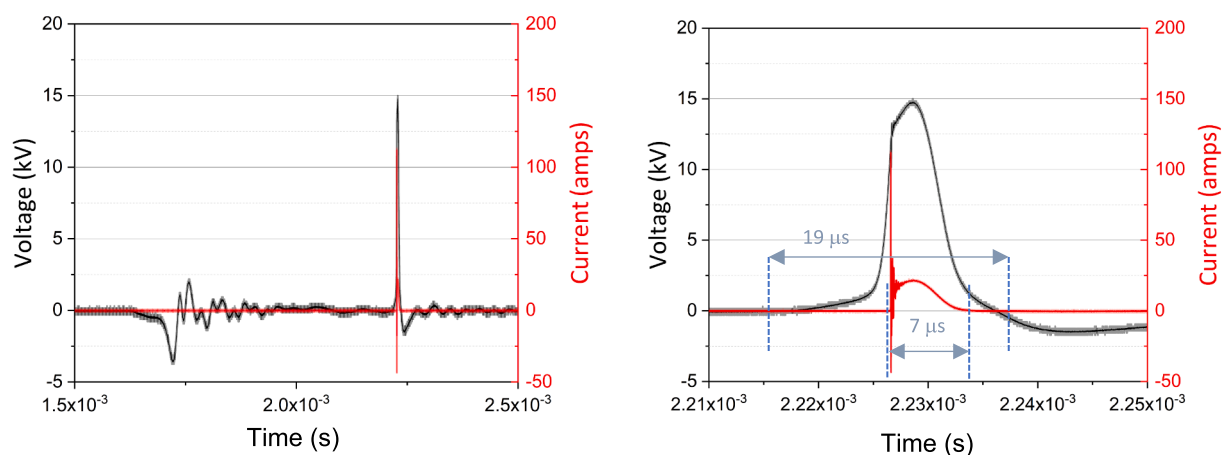

Fig. 5. The voltage (black) and current (red) waveform applied to the discharge electrode by the KAM power supply over an entire single pulse of energy (left) and a magnified view of the waveform to visualise the short duration of the current discharge peaks (right).

rectangular reactor), the superficial velocity for the 25 L reactor was 2.2 cm/min, while in contrast, the reactor in Singh et al. used a higher superficial velocity of 5.0–5.6 cm/min. Optimising the sparger to favour fine bubble size, transport of PFAS to the surface and fluid dynamics in the developed reactor allowed for the use of lower argon superficial velocities. These improvements may be beneficial for reducing the operating and capital costs for larger scale operations, as it reduces the overall volume of argon gas used and the size of the compressors or blowers used to supply the gas into the reactor or to recycle the argon. Other published studies indicate EE/O values of 5.5 kWh/m^3 and values over 100 kWh/m^3 though it should be noted that these are for significantly higher concentrations of PFAS [38,39], and other factors such as PFAS species and water chemistry also play a significant role on the energy required for remediation.

The time constant compares favourably with our previous work at the 2 L scale, where most similar experiment had a rate constant of 0.11 min^{-1} [24]. A recent study had a rate constant of 0.4 min^{-1}, though this was in a 1.5 L reactor with added CTAB [40].

As seen in the four graphs shown in Fig. 7, the concentration of PFSA compounds, such as PFHxS and PFHpS slowly decreased over time, falling below detectable concentrations (< 0.01 µg/L) typically after 60 min and 40 min, respectively. Achieving high destruction rates of these shorter-chain PFSA is particularly crucial as PFHxS is one of the three regulated PFAS, along with PFOS and PFOA, with drinking and recreation water guideline values defined by the NHMRC [32].

However, the concentrations of these key species at sampling point A exceeded the drinking water values defined by the NHMRC with a total of 0.98 µg/L of PFHxS (0.08 µg/L) and PFOS (0.90 µg/L) detected at this sampling point. The variability in PFAS concentration across samples at varying heights throughout the bulk of the liquid or from the liquid surface raises an interesting conundrum of how the sampling position and depth within a liquid can result in water meeting discharge of drinking water standards because of the tendency for surface active PFAS to accumulate at the surface.

3.3. Bubble size distributions and mass transfer rates

The $k_L a$ was readily determined for the two spargers and the results are shown in Table 1. below, as the average of three repeats and the range being given by the highest and lowest values obtained for each sparger. Equivalent Sauter Mean Diameters were then estimated for these mass transfer rates, using the bubbles measured rise velocity and liquid film mass transfer coefficients from the work of Motarjemi and Jameson [27].

Both the photographic approach and the spectroscopic bubble sizing method yielded different bubble size distributions due largely to the Dantec probe being able to detect bubbles as small as 0.02 mm. The peak in bubble size for the ECD sparger as ~ 0.2 mm which was the limit for the photographic technique.

Fig. 6 shows the results of photographic analysis and the Dantec probe of bubbles generated from both the disc-shaped, medium bubble

Table 1
Summary of Mass Transfer and Bubble Diameter Estimates.

	Fine bubble (ECD200)	Medium bubble (Corundum)
$k_L a$ (s^{-1})	0.0081±0.0007	0.0026±0.0003
d_{eq} (mm) based on $k_L a$	0.60–0.8	1.4–2.2
d_{32} (mm) Photographic	1.5	3.8
d_{32} (mm) Dantec Shadow Statistics	0.81–1.00	1.39–1.42
d_{32} (mm) Dantec Adaptive Shadow Tracking	1.15–1.20	1.62–1.84
d_{32} (mm) Dantec corrected*	0.76–0.90	NA

* Corrected d_{32} for the fine bubble diffuser excluded large bubbles observed to form on the probe.

diffuser (Corundum) and the annular-shaped, fine bubble diffuser (ECD200). The frequency of the 0.1 to 3.0 mm diameter bubbles produced by the fine bubble diffuser (left axis, black) and the 0.1 to 6.0 mm bubbles produced by the medium bubble diffuser (right axis, red) are shown in Fig. 6. This figure is based on the characterisation of 17,214 and 3,189 bubbles identified for the fine and medium bubble diffuser, respectively, using the photographic method. For the Dantec probe the figure is based on 20,000–30,000 bubbles for the fine and 10,000–12,000 for the medium bubble diffuser. The figure presents the projected bubble diameter assuming spherical bubbles.

Around 90% of the 17,214 bubbles analysed from the fine bubble diffuser images were ≤ 1.0 mm in diameter, with a median bubble size of 0.5 mm. The remaining $\sim 10\%$ of bubbles were in the 1.1–3.0 mm range, which included some bubbles that were abnormally large due to coalescence occurring due to the imaging approach which physically divided the total output of bubbles from the diffuser using an opaque sheet, thereby providing a surface for some bubbles to coalesce. All the bubbles produced by this diffuser were spherical, and no bubbles produced by this diffuser were found to exceed 3.0 mm in diameter.

The randomised nature of the medium bubble diffuser contains a range of pore sizes, producing a much broader distribution of bubble sizes at lower operating pressures at effectively the pressure induced by the liquid pressure (~ 0.2 bar). The formation of larger bubbles, 3.0–6.0 mm, was more prevalent with this diffuser as some bubbles could form on the underside, resulting in them coalescing as they were forced against the bottom of the tank and underneath the diffuser.

The results obtained with the Dantec spectroscopic probe revealed a substantial number of small bubbles that were not captured by the photographic method. The fine bubble diffuser had 5% of total bubbles below 0.05 mm, 20% below 0.1 mm and 50–60% below 0.21 mm. Surprisingly the medium bubble diffuser had 5–10% of the total bubble count below 0.2 mm.

The smaller bubbles produced from the fine bubble diffuser had a bubble surface area of 0.139–0.167 m^2 per 1 L of gas flow compared with only 0.047–0.053 m^2 by the medium bubble diffuser, which is effectively only one third of the total bubble surface area produced by the fine bubble diffuser at the same volumetric flow.

The Sauter Mean Diameter (SMD) measured for the fine bubble sparger was smaller than the photographic method, though there were still issues with stray large bubbles caused by the placement of the probe which inflated both the calculated value of the SMD for both the "Shadow Statistics" and "Adaptive Shadow Tracking" results. Excluding large bubbles of 2 mm or greater from the "Adaptive Shadow Tracking" results in closer values to those estimated from $k_L a$, hence these bubbles, which are an artefact of the probe being placed on an angle into the column, are the likely cause of the discrepancy.

For the medium bubble sparger, the utilised software often did not identify ellipsoid bubbles when they first entered the field of view but did after several frames. Hence the "Shadow Statistics" measurement was lower than the Adaptive Shadow Tracking method. The Adaptive Shadow Tracking method likely also have underestimated the SMD, due to some smaller bubbles being given more than one ID number by the software when eclipsed by larger bubbles, however this effect appears to be small and the obtained values are only slightly lower than the $k_L a$ based values.

3.4. Comparison of breakdown kinetics

The rate constants calculated for PFOS degradation over the first 40 min of plasma treatment were used to compare the breakdown kinetics for the fine and medium bubble diffusers. Only the first 40 min of data were used to determine the rate constants as the regression lines for the logarithm of concentration versus time were highly linear over this period ($r^2 = 0.97$–0.99) and when including time beyond this, the very high conversions approaching 100% skewed the data, reducing the fit of
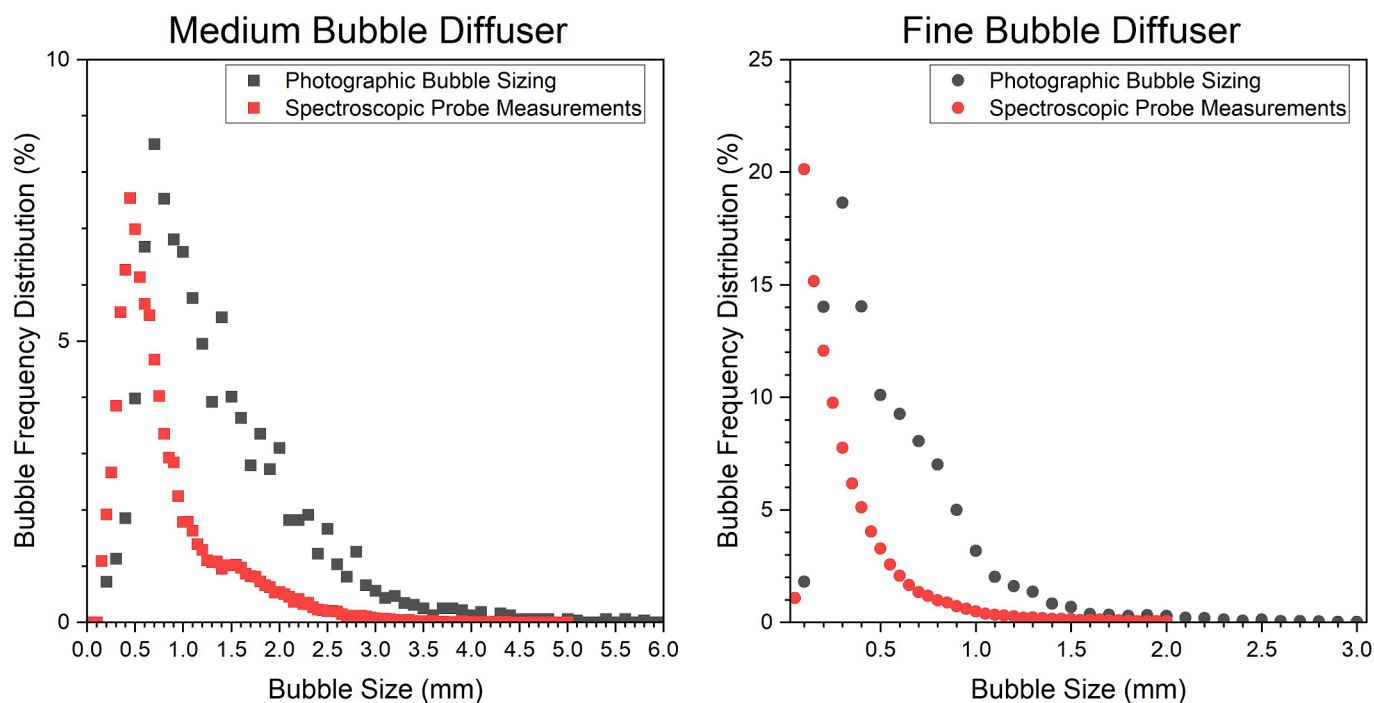
Fig. 6. Frequency of each bubble size (mm) produced by the disc shaped, medium bubble diffuser, left panel and the fine diffuser (right panel) as measured by photographic and Dantec Spectroscopic probes.
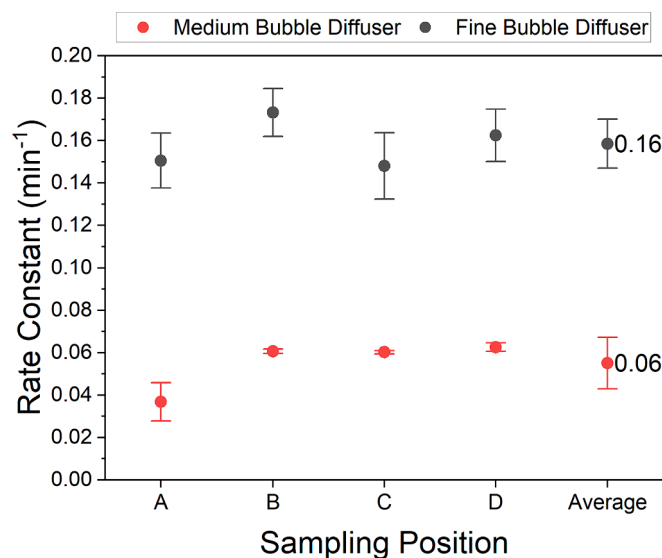

Fig. 7. Comparison of the rate constants calculated at each sampling position for the breakdown of PFOS when operating with the fine and medium bubble diffusers. Rate constants were calculated at each sampling point, with the average of the four points presented on the far right.

the regression lines ($r^2 < 0.60$). The rate constant for PFOS was used as a metric to compare the results as it was the primary PFAS compound detected in both experiments, accounting for $> 90\%$ of the initial PFAS concentration and was the principal compound that underwent degradation. The breakdown was found to satisfy the equation below, which describes the pseudo-first order breakdown kinetics:

$$\frac{d[PFOS]}{dt} = -k_b[PFOS] \qquad (4)$$

The rate constant k_b is determined by several phenomena, including the

surface activity, the available bubble surface area, plasma input power and the surface renewal of the liquid due to agitation induced by the bubbles. The data describing the conversion (X) for PFOS were used to calculate the rate constants equal to the gradient of the line from the linear regression of $-\ln(1-X)$ against time at each concentration investigated. Additionally, due to its high surfactant strength compared with the other products detected in the solution, PFOS would competitively be adsorbed to the gas–liquid interface and hence would be the dominant PFAS floated to the surface and interfaced with the plasma [41].

The rate constants were calculated at each sampling point, with the average values determined to be 0.16 ± 0.01 min^{-1} for the fine bubble diffuser and 0.06 ± 0.003 min^{-1} for the medium bubble diffuser, as shown in Figure. The rate constant for PFOS degradation using the fine bubble diffuser was around 290% higher than the average rate constant determined for the medium bubble diffuser. The stark difference in the calculated rate constants demonstrates the significant benefits of using diffusers that produce smaller bubbles for a batch system and the relative values are in a similar ratio to the measured values.

These rate constants are the change in concentration, including the destruction of PFAS and any reduction in concentration due to the transport of PFAS to the surface. Therefore, the rate constants presented here are a combination of both phenomena: destruction and floatation, as these two contribute in the non-thermal plasma bubble column to reduce the concentration of the PFAS.

The large bubble surface area produced by the fine bubble diffuser is highly effective at floating and accumulating the PFAS at the liquid surface for destruction in the batch reactor trialled here. However, when considering a continuous flow treating reactor, the addition of the hydrodynamic mixing caused by the larger bubbles from a medium bubble diffuser may be deemed more beneficial for promoting the mixing between a fresh inlet stream and the bulk of the reactor volume. Additionally, the higher pressures required to operate the fine bubble diffuser (~1.5 bar) would require larger-scale treatment reactors to be built as a pressure vessel to withstand these pressures, adding additional capital expenditure to ensure safety. Therefore, although the fine bubble diffuser significantly improves the breakdown rate of PFAS in the batch

mode, the non-thermal plasma bubble column developed here may not be ideal for future, larger-scale reactors due to the engineering design favouring safety and more economical options.

3.5. One dimensional Mathematical model of PFOS removal

Given the correlation between the $k_L a$ values and the observed time constants for destruction, and that previous workers have identified such behaviour as characteristic of mass transfer limitation, a relatively simple one-dimensional mass transfer model was developed to determine if the rate of PFAS breakdown was predictable.

3.5.1. Model assumptions

The premise of the model is that the dynamical behaviour of the bubbles can be predicted based on their terminal velocity and the speed of the liquid flow and that mass transfer is limited by diffusion to the bubble interface until that interface becomes saturated. The key model features and inputs are presented in Fig. 8.

The following assumptions were made to develop the model:

- Plasma discharge covers most of the top surface of the reactor and the breakdown of PFOS is limited by its rate of convective transport by bubbles to the argon-water interface.
- The SMD can approximate the behaviour of the bubble size distribution, with no breakup or coalescence occurring as they rise.
- The bubble volume fraction is low ~ 1% and they are in the homogeneous regime.
- Bubbles rise at a constant velocity based on the SMD corrected for the induced water flow.
- Bubbles leave the PFOS at the surface when they break and all PFOS transported to the surface is broken down.
- Bubble rise is relatively fast compared with the rate of change the bulk liquid concentration.
- The bubble rise velocity can be modelled using Clift et al.'s contaminated bubble curve, applicable as the water is contaminated by many species [25].

- Mass transfer can be modelled by Motarjemi and Jameson's work for oxygen diffusion as a function of bubble size, as these data cover the conditions observed here, and the molecule size effect can be corrected for via the Schmidt number [25].
- The maximum loading of PFOS on bubbles is represented using a K_{equil} value of 23×10^{-6} m, which is multiplied by an enhancement of 74 for the presence of calcium applied to the model of Brusseau and Glubt [26].
- Bubbles enter the column with no PFAS on their surface.
- Other species are not considered due to PFOS being the dominant species for the initial stages of the experiments and being highly surface active.

3.5.2. Model formulation

In this section we develop the equations in a step-by-step manner, making use of the assumptions given above. It is assumed that the PFAS mass concentration in the bulk is sufficiently low that the equilibrium at the bubble surface can be given by

$$C_{\text{surf}} = C_{\text{bl}} K_{\text{equil}} \tag{5}$$

By definition, the mass transfer rate to a single bubble is given by:

$$\frac{dm_b}{dt} = k_L A_b (C_\infty - C_{\text{bl}}) \tag{6}$$

The bubble concentration in the liquid at the bubble surface can be eliminated using eq. (5), to give:

$$\frac{dm_b}{dt} = k_L A_b \left(C_\infty - C_{\text{surf}} / K_{\text{equil}} \right) \tag{7}$$

By definition

$$C_{\text{surf}} = m_b / A_b \tag{8}$$

so that C_{surf} can be eliminated to give:

Hydrodynamics

Argon bubbles enter via sparger with no attached PFAS.

Bubbles rapidly attain their terminal velocity relative to the fluid bulk flow induced by the gas flow.

Bubble residence time is calculable from the liquid depth divided by this bubble speed.

Inputs

Gas flow rate.

Bubble size.

Terminal velocity correlation.

Liquid speed.

Mass Transfer

Controlled by species convection/diffusion to the bubble surface modeled by a Henry Isotherm.

Adsorption capacity at surface depends on molecular properties and other species present.

Inputs

Equilibrium constant.

Solution composition to determine effective equilibrium constant.

Mass transfer correlation.

Diffusion coefficients.

PFAS Destruction

Entire surface is covered by plasma.

All PFAS on bubbles is released at the surface.

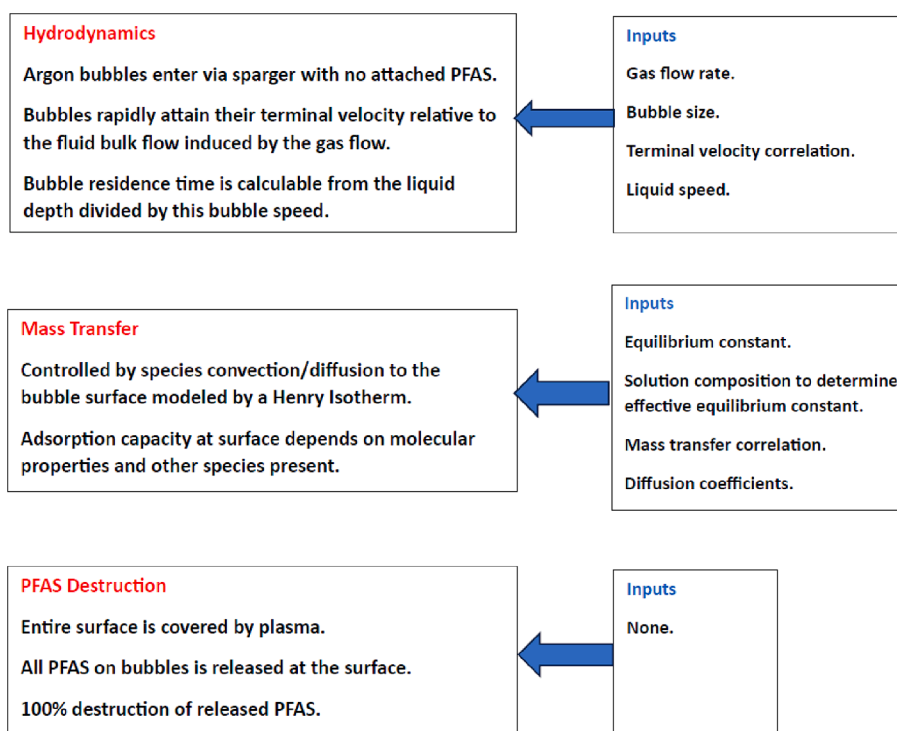100% destruction of released PFAS.

Inputs

None.

Fig. 8. Schematic representation of the model of the model assumptions and required inputs.

$$\frac{dm_b}{dt} = k_L A_b \left(C_\infty - \frac{m_b}{(K_{\text{equil}} A_b)} \right) \tag{9}$$

The transit time of a bubble from injection at the sparger to the free surface is simply the liquid height divided by the bubble rise velocity. The latter can be broken down into the sum of the bulk upward flow of the liquid (obtained from bubble size measurement data and CFD simulations) plus the bubble terminal velocity, so that:

$$t_{\text{rise}} = H/(u_L + u_b) \tag{10}$$

The number of bubbles present in the column is the volumetric flowrate of gas multiplied by the rise time divided by the volume of a single bubble:

$$N_{bt} = 6\dot{V}_G t_{\text{rise}}/\pi d^3 \tag{11}$$

Using the above relationships, the mass of PFOS carried by the swarm of bubbles can be calculated using:

$$\frac{dm_s}{dt} = N_{bt} k_L A_b \left(C_\infty - \frac{m_s}{(K_{\text{equil}} N_{bt} A_b)} \right) \tag{12}$$

The PFAS concentration in the vessel can be estimated by assuming perfect mixing, so that:

$$C_\infty = C_0 - \frac{m_s}{V} \text{ for } t < t_{\text{rise.}} \tag{13}$$

Differentiating with respect to time gives the change in bulk concentration over time:

$$\frac{dC_\infty}{dt} = -\frac{N_b k_L A_b}{V} \left(C_\infty - \frac{V(C_0 - C_\infty)}{(K_{\text{equil}} N_{bt} A_b)} \right) \tag{14}$$

Equation (14) can be solved using time integration with the initial condition $C_\infty(0) = C_0$. Details of the solution method are given in the python code given in the Supplementary data. Once the solution is obtained, it is straightforward to determine the average rate constant over the rise time, which gives the average pickup rate of PFOS by a swarm of bubbles and by assuming complete destruction by the plasma this can be compared with the experimental value. In this work a numerical approach has been used to solve the diffusion equations, making use of the known initial conditions. Li et al. developed a similar method to solve the equation of Ward and Tordai, for the diffusion limited mass transfer of a non-ionic surfactant to a bubble surface [42,43].

3.6. Constitutive models

3.6.1. Bubble terminal velocity

Clift et al. have a graph showing the rise velocity of a bubble in both clean and contaminated water. The rise velocity of bubbles is the same for clean and contaminated water for bubbles up to 0.5 mm, and then is lower for contaminated water for bubble sizes to 20 mm [25].

For bubbles d_b of 0.2 to 4 mm the velocity u_b in m/s is well fitted by:

$$u_b = \frac{0.5293 d_b^3 - 4.9437 d_b^2 + 15.901 d_b - 1.4029}{100} \tag{15}$$

This terminal velocity is used to estimate the velocity of the bubble travelling through water containing PFAS.

Motarjemi and Jameson [27] have a slightly higher rise velocity for small bubbles in clean water, particularly for London Tap Water which is relatively hard. For d_b between 0.2 and 3 mm the terminal velocity in m/s is well fitted by:

$$u_b = \frac{0.0296 d_b^3 - 3.4936 d_b^2 + 17.989 d_b - 1.3111}{100} \tag{16}$$

Motarjemi and Jameson's velocity is used to compare with the measured velocities from the Dantec probe to estimate the velocity of the water/bubble swarm, given the hard water present in the Danish laboratory where the experiments were performed.

3.6.2. Mass transfer coefficients

Motarjemi and Jameson present k_L data for oxygen water transfer in cm/s that for $d_b < 2.4$ mm can be used to estimate k_L for PFOS in m/s by the ratio of the diffusivities of PFOS and oxygen in water to the power of 2/3 [27].

$$k_L = \frac{\left(-0.0014 d_b^3 - 0.0038 d_b^2 + 0.0378 d_b - 0.0019 \right)}{100} \times \left(\frac{0.49}{2} \right)^{\frac{2}{3}} \tag{17}$$

3.6.3. Modelling results

The above model was applied to the PFOS breakdown experiments described above. The inputs used are given in Table 2. The model was developed in python to integrate eq. (14) over the rise time (eq. (10)) to yield the effective breakdown rate. The model was then used to explore the impact of uncertain inputs, such as bubble size. A range of bubble sizes was considered for each sparger, based on the data from Table 1 and the analysis presented in the supplementary data.

The results presented in Table 3 show that the model can capture the breakup trend between the two spargers. For the fine sparger the predicted results fall inside the experimental uncertainty band. For the medium sparger the results fall below the experimental range but using a slightly smaller bubble size (1.2 mm) and/or a lower bulk velocity (0.1 m/s) of the liquid would bring them well inside the experimental range.

4. Conclusions

An increase of 290% in the rate constant calculated for PFOS breakdown during plasma treatment was observed when using the fine bubble producing ECD200 diffuser (0.16 ± 0.01 min^{-1}) compared with the corundum disc diffuser (0.06 ± 0.003 min^{-1}). This difference is similar to the ratio of the $k_L a$ values for the spargers of 0.0081 ± 0.0007 s^{-1} versus 0.0026 ± 0.0003 s^{-1}.

The smaller bubbles produced by the ECD200 diffuser provided a larger surface area to float PFAS to the surface for plasma treatment, more than double compared with the corundum disc diffuser. A simple model was able to predict the removal rate constants for both spargers using measured parameters and well-established correlations to within $\pm 30\%$.

Significant concentration gradients of PFOS were found when sampling from different liquid heights within the 25 L reactor, particularly when utilising a smaller bubble size distribution. Liquid samples taken from the liquid surface contained 200 to 300% higher concentrations of PFOS compared with samples from the bulk of the reactor volume. The sampling position has emerged as an important sampling consideration as it significantly influences determinisation of the composition and overall breakdown rate within a treatment reactor, which is particularly important for benchmarking and comparing treatment reactor designs.

Electrical diagnostics of the power supplied by the KAM industrial power supply to the high voltage electrode showed very short current durations of 7 μs per pulse which resulted in very energy-efficient use of power and 216.3 ± 6.6 W of power consumed by the plasma discharge. An EE/O parameter of 2.0 ± 0.1 kWh/m^3 was calculated for reducing

Table 2
Inputs used in the modelling.

Quantity	Value
Argon flow rate (L/min)	1
Liquid depth (m)	0.58
Liquid volume (m^3)	0.026
Equilibrium constant (m)	0.001702

Table 3
Results of the 1 D model for PFOS using the fine or medium bubble diffusers.

Quantity	Unit	Fine		Medium	
d_b	mm	0.6	0.8	1.4	2.2
k_{L,O_2}	m/s	1.91×10^{-4}	2.52×10^{-4}	3.97×10^{-4}	4.80×10^{-4}
$k_{L,PFOS}$	m/s	7.48×10^{-5}	9.86×10^{-5}	1.56×10^{-4}	1.88×10^{-4}
u_b	m/s	0.065	0.084	0.126	0.153
u_L	m/s	0.01	0.01	0.15	0.15
k	min^{-1}	0.157	0.120	0.0424	0.0284
k(exp)	min^{-1}	0.16+/−0.01		0.06+/−0.003	

the concentration of PFOS by 90% in 1 m^3 of contaminated water utilising the fine bubble diffuser, whereas much high values of 8.4 ± 2.5 kWh/m^3 were calculated for the medium bubble diffuser. The EE/O values demonstrate that the treatment reactor has a high efficiency at treating PFOS which are comparable with values in the literature, whilst using only 1% of the argon gas flow of other similar plasma treatment reactor designs. Whilst smaller bubbles were found to improve the mass transfer process and overall destruction in a batch system, care should be taken for designing continuous systems where carryover would be a concern.

CRediT authorship contribution statement

David Alam: Writing – review & editing, Writing – original draft, Investigation, Formal analysis, Data curation, Conceptualization. **Samiuela Lee:** Validation, Methodology, Formal analysis, Data curation. **Jungmi Hong:** Methodology, Investigation, Formal analysis. **David F. Fletcher:** Writing – review & editing, Supervision, Software, Methodology, Funding acquisition, Formal analysis. **Xinying Liu:** Writing – review & editing, Visualization, Software. **Dale McClure:** Writing – review & editing, Methodology, Funding acquisition, Conceptualization. **David Cook:** Writing – review & editing, Writing – original draft, Investigation, Formal analysis, Data curation, Conceptualization. **Johan le Nepvou de Carfort:** Writing – review & editing, Software, Methodology, Investigation, Data curation. **Ulrich Krühne:** Writing – review & editing, Supervision, Resources. **P.J. Cullen:** Writing – review & editing, Supervision, Resources, Funding acquisition, Conceptualization. **John M. Kavanagh:** .

Declaration of competing interest

The authors declare the following financial interests/personal relationships which may be considered as potential competing interests: John Kavanagh reports financial support was provided by The University of Sydney. John Kavanagh reports financial support and equipment, drugs, or supplies were provided by ICD Asia Pacific. John Kavanagh reports financial support was provided by ICD Asia Pacific. John Kavanagh, PJ Cullen, Dale McClure reports financial support was provided by Australian Research Council. David Alam reports financial support was provided by The University of Sydney. PJ Cullen reports a relationship with Plasma Leap that includes: equity or stocks. PJ Cullen has patent pending to PlasmaLeap. If there are other authors, they declare that they have no known competing financial interests or personal relationships that could have appeared to influence the work reported in this paper.

Data availability

Data will be made available on request.

Appendix A. Supplementary data

Supplementary data to this article can be found online at https://doi.org/10.1016/j.cej.2024.151349.

References

[1] EPA – United States Environmental Protection Agency. PFAS Master List of PFAS Substances. https://comptox.epa.gov/dashboard/chemical_lists/pfasmaster.
[2] C.M. Sharts, Organic fluorine chemistry, J. Chem. Educ. 45 (1968) 185.
[3] E. Kissa, Fluorinated surfactants and repellents, Marcel Dekker, 2001.
[4] K. Jansen, 'Forever chemicals' no more? C&EN Glob. Enterp. 97 (2019) 28–32.
[5] J.P. Giesy, K. Kannan, Global distribution of perfluorooctane sulfonate in wildlife, Environ. Sci. Tech. 35 (2001) 1339–1342.
[6] G.L. Lescord, et al., Perfluorinated and polyfluorinated compounds in lake food webs from the Canadian High Arctic, Environ. Sci. Tech. 49 (2015) 2694–2702.
[7] K. Hoffman, et al., Perfluorooctanoic Acid Exposure and Cancer Outcomes in a Contaminated Community: A Geographic Analysis, Environ. Health Perspect. 121 (2013) 318–323.
[8] C8 Science Panel. C8 Probable Link Reports. http://www.c8sciencepanel.org/prob_link.html (2012).
[9] K. Steenland, L. Zhao, A. Winquist, C. Parks, Ulcerative colitis and perfluorooctanoic acid (PFOA) in a highly exposed population of community residents and workers in the Mid-Ohio Valley, Environ. Health Perspect. 121 (2013) 900–905.
[10] D.J. Burns, P. Stevenson, P.J.C. Murphy, PFAS removal from groundwaters using Surface-Active Foam Fractionation, Remediation 31 (2021) 19–33.
[11] J. Thompson, et al., Removal of PFOS, PFOA and other perfluoroalkyl acids at water reclamation plants in South East Queensland Australia, Chemosphere 82 (2011) 9–17.
[12] C.G. Pan, Y.S. Liu, G.G. Ying, Perfluoroalkyl substances (PFASs) in wastewater treatment plants and drinking water treatment plants: Removal efficiency and exposure risk, Water Res. 106 (2016) 562–570.
[13] Psillakis, E., Hoffmann, M. R., Colussi, A. J. & Cheng, J. Enrichment Factors of Perfluoroalkyl Anionic Surfactants at the Air / water Interface. **11**, 11179 (2009).
[14] C. Nau-Hix, T.M. Holsen, S. Mededovic Thagard, Optimization of a gas–liquid plasma reactor for water treatment applications: Design guidelines and electrical circuit considerations, Plasma Process. Polym. 19 (2022) 2200036.
[15] P. Stevenson, S.I. Karakashev, Commercial-scale removal of short-chain PFAS in a batch-wise adsorptive bubble separation process by dosing with cationic co-surfactant, Remediat. J. 34 (2024).
[16] R.P. Joshi, S.M. Thagard, Streamer-Like Electrical Discharges in Water: Part II. Environmental Applications, Plasma Chem. Plasma Process. 33 (2013) 17–49.
[17] B.R. Locke, M. Sato, P. Sunka, M.R. Hoffmann, J.S. Chang, Electrohydraulic discharge and nonthermal plasma for water treatment, Ind. Eng. Chem. Res. 45 (2006) 882–905.
[18] L. Huang, W. Dong, H. Hou, Investigation of the reactivity of hydrated electron toward perfluorinated carboxylates by laser flash photolysis, Chem. Phys. Lett. 436 (2007) 124–128.
[19] X. Liu, et al., Photochemical decomposition of perfluorochemicals in contaminated water, Water Res. 186 (2020).
[20] N. Takeuchi, et al., Plasma-liquid interfacial reaction in decomposition of perfluoro surfactants, J. Phys. D Appl. Phys. 47 (2014).
[21] M. Vasilev, P. Conlon, D. Bohl, S.M. Thagard, The Effect of Discharge Frequency of a Gas-Liquid Plasma Reactor on Bulk Liquid Transport and Removal of Organic Contaminants, Plasma Chem. Plasma Process. 42 (2022) 759–783.
[22] S. Mededovic Thagard, et al., Plasma-based water treatment: development of a general mechanistic model to estimate the treatability of different types of contaminants, J. Phys. D Appl. Phys. 50 (2017) 014003.
[23] G.P. Lucas, R. Mishra, Measurement of bubble velocity components in a swirling gas-liquid pipe flow using a local four-sensor conductance probe, Meas. Sci. Technol. 16 (2005) 749–758.
[24] D. Alam, et al., Experimental investigations of Per- and Poly-fluoroalkyl Substances (PFAS) degradation by non-thermal plasma in aqueous solutions, J. Environ. Chem. Eng. 111588 (2023), https://doi.org/10.1016/j.jece.2023.111588.
[25] Clift, R. (Roland), Grace, J. R. & Weber, M. E. Bubbles, drops, and particles . (Academic Press, 1978).
[26] M.L. Brusseau, S. Van Glubt, The influence of surfactant and solution composition on PFAS adsorption at fluid-fluid interfaces, Water Res. 161 (2019) 17–26.
[27] M. Motarjemi, G.J. Jameson, Mass transfer from very small bubbles—the optimum bubble size for aeration, Chem. Eng. Sci. 33 (1978) 1415–1423.

[28] N. Frössling, Über die verdunstung fallender tropfen, Gerlands Beiträge Zur Geophys. 52 (1938) 170–216.

[29] P.H. Calderbank, M.B. Moo-Young, The continuous phase heat and mass-transfer properties of dispersions, Chem. Eng. Sci. 16 (1961) 39–54.

[30] R.W. Higbie, The Rate of absorption of a pure gas into a still liquid during short periods of exposure, Transactions of the American Institute of Chemical Engineers 31 (1935) 365–389.

[31] NSW Health. PFOS and PFOA - Fact sheets. https://www.health.nsw.gov.au/environment/factsheets/Pages/pfos.aspx.

[32] National Health and Medical Research Council, National Resource Management Ministerial Council & Commonwealth of Australia, C. *NHMRC, NRMMC (2011) Australian Drinking Water Guidelines Paper 6 National Water Quality Management Strategy*. (2011).

[33] P.H.N. Vo, et al., Foam fractionation of per- and polyfluoroalkyl substances (PFASs) in landfill leachate using different cosurfactants, Chemosphere 310 (2023) 136869.

[34] R.K. Singh, E. Brown, S. Mededovic Thagard, T.M. Holsen, Treatment of PFAS-containing landfill leachate using an enhanced contact plasma reactor, J. Hazard. Mater. 408 (2020) 124452.

[35] R.K. Singh, et al., Removal of Poly- And Per-Fluorinated Compounds from Ion Exchange Regenerant Still Bottom Samples in a Plasma Reactor, Environ. Sci. Tech. (2020), https://doi.org/10.1021/acs.est.0c02158.

[36] J.R. Bolton, K.G. Bircher, W. Tumas, C.A. Tolman, Figures-of-merit for the technical development and application of advanced oxidation technologies for both electric- and solar-driven systems, Pure Appl. Chem. 73 (2001) 627–637.

[37] R.K. Singh, et al., Rapid Removal of Poly- and Perfluorinated Compounds from Investigation-Derived Waste (IDW) in a Pilot-Scale Plasma Reactor, Environ. Sci. Tech. (2019), https://doi.org/10.1021/acs.est.9b02964.

[38] D. Zhu, et al., Reactive Nitrogen Species Generated by Gas-Liquid Dielectric Barrier Discharge for Efficient Degradation of Perfluorooctanoic Acid from Water, Environ. Sci. Tech. 56 (2022) 349–360.

[39] H. Zhang, et al., Enhancing Interface Reactions by Introducing Microbubbles into a Plasma Treatment Process for Efficient Decomposition of PFOA, Environ. Sci. Tech. 55 (2021) 16067–16077.

[40] R. Li, O.F. Isowamwen, K.C. Ross, T.M. Holsen, S.M. Thagard, PFAS-CTAB Complexation and Its Role on the Removal of PFAS from a Lab-Prepared Water and a Reverse Osmosis Reject Water Using a Plasma Reactor, Environ. Sci. Tech. 57 (2023) 12901–12910.

[41] M.L. Brusseau, S. Van Glubt, The influence of molecular structure on PFAS adsorption at air-water interfaces in electrolyte solutions, Chemosphere 281 (2021) 130829.

[42] A.F.H. Ward, L. Tordai, Time-dependence of boundary tensions of solutions I. The role of diffusion in time-effects, J. Chem. Phys. 14 (1946) 453–461.

[43] X. Li, R. Shaw, G.M. Evans, P. Stevenson, A simple numerical solution to the Ward-Tordai equation for the adsorption of non-ionic surfactants, Comput. Chem. Eng. 34 (2010) 146–153.